Probing the Room Temperature Spatial Distribution of Hydrogen in Nanoporous Carbon by Use of Small-Angle Neutron Scattering

Cheng-Si Tsao,[†,‡] Mingda Li,[†] Yang Zhang,[†,||] Juscelino B. Leao,[§] Wei-Shan Chiang,[†] Tsui-Yun Chung,[‡] Yi-Ren Tzeng,[‡] Ming-Sheng Yu,[‡] and Sow-Hsin Chen*[,†]

Department of Nuclear Science and Engineering, Massachusetts Institute of Technology, Cambridge, Massachusetts 02139, United States, Institute of Nuclear Energy Research, Longtan, Taoyuan 32546, Taiwan, NCNR, National Institute of Standard and Technology, Gaithersburg, Maryland 20899, United States, and Neutron Scattering Science Division and Joint Institute for Neutron Sciences, Oak Ridge National Laboratory, Oak Ridge, Tennessee 37831, United States

Received: June 15, 2010; Revised Manuscript Received: September 28, 2010

The spatial distribution of hydrogen physically adsorbed in a nanoporous carbon at room temperature (RT) as a function of H_2 gas pressure is investigated for the first time using small-angle neutron scattering (SANS). A hierarchical pore structure consisting of micropores and a fractal mesopore network of the used activated carbon is also studied to correlate the relationship between the spatial distribution of hydrogen and the pore confinement. The cylinder-like cluster of aggregated hydrogen is formed and is confined in the disklike micropore. The evolution of spatial structures of adsorbed hydrogen with hydrogen pressure is elucidated. A direct experimental observation of the spatial distribution and the behavior of hydrogen adsorbed in the porous materials at RT is still scarce to date. The analysis results obtained by SANS provide new information for the future investigations of the RT storage mechanism of hydrogen in the nanoporous materials developed for the purpose of on-board hydrogen storage.

Introduction

Hydrogen storage plays a crucial role in the development of sustainable energy applications to fuel cell-based vehicles. Microporous carbon as an adsorbent is the most attractive candidate for hydrogen storage due to its low weight, high stability, and low cost.[1−7] According to the target criteria of the U.S. Department of Energy (DOE), the on-board hydrogen storage needs to be reversible at ambient temperature and at pressures less than 10 MPa. Because of its low binding energy to H_2, porous carbon adsorbent typically has small storage capacity at room temperature (RT).[2−4,7] Fundamental understanding of hydrogen fuel gas stored in carbon nanopores with right pore size (less than 2 nm by definition) at RT is not yet forthcoming and has been the focus of theoretical simulations.[7−10] Hence, further experimental studies are critical to develop the porous materials with large RT hydrogen storage capacity. Hydrogen adsorbed in carbon nanopores at RT may be explained by the micropore filling mechanism.[11] However, the experimental observation of the pore filling mechanism in the porous carbon is very limited at the atomic and nanometer scale. On the other hand, the physisorbed hydrogen molecules in the nanopores at RT may tend to form a specific structure favorable for both the molecule surface and the intermolecular interactions.[12−14] The complicated pore structure of the typical activated carbon (AC) further increases the difficulties of the research.[15,16] The relation between the confinement structure and the adsorption behavior of hydrogen at RT is an interesting and a fundamental research topic. Small-angle neutron scattering (SANS) is a powerful tool to investigate both the nanostructure of adsorbed hydrogen and the pore structure of AC from nanoscale to mesoscale.[3,16] This study employed the SANS technique for the first time to study the spatial distribution of the hydrogens physically adsorbed in a nanoporous carbon at RT and its structural evolution as a function of hydrogen gas pressure.

The structure and behavior of gas fuel or other gases adsorbed or confined in carbon nanospaces at high pressure have attracted much interest.[11−14] However, an X-ray small angle scattering study on the nanoscale structure of hydrogen at this situation has never been reported due to its low atomic number. Because there is a large neutron scattering cross-section for hydrogen,[17,18] the current work employed SANS to resolve the structure of physisorbed hydrogen at RT in an AC sample. It has been shown by many theoretical literatures that the pore size in an AC sample is the key factor for H_2 adsorption at RT. The pore size is closely related to the binding energy calculated[7−10] and is also considered as the design parameters for optimized hydrogen storage material.[9] On the basis of the SANS data, our current study proposes a possible three-dimensional (3D) packing model of hydrogen molecules adsorbed in the nanopores of AC. Our data seem to show the evidence of the evolution of adsorbed hydrogen molecules clusters on the carbon surface as a function of hydrogen pressure. Our results are helpful to study the adsorption mechanism at RT in amorphous carbon materials for the further optimization of materials for RT hydrogen storage.

Nitrogen isotherm analysis traditionally used for pore size characterization has several drawbacks, such as the reliance of a model for pore geometries.[19] In contrast, SANS characterization can independently provide the information of the pore sizes and geometries of the various pores in AC and their spatial distribution. In the current paper, the combined study of nitrogen isotherm and SANS technique is first performed to accurately

* To whom correspondence should be addressed. E-mail: sowhsin@mit.edu.
[†] Massachusetts Institute of Technology.
[‡] Institute of Nuclear Energy Research.
[§] National Institute of Standard and Technology.
[||] Oak Ridge National Laboratory.

10.1021/jp1055039
Published on Web 11/09/2010

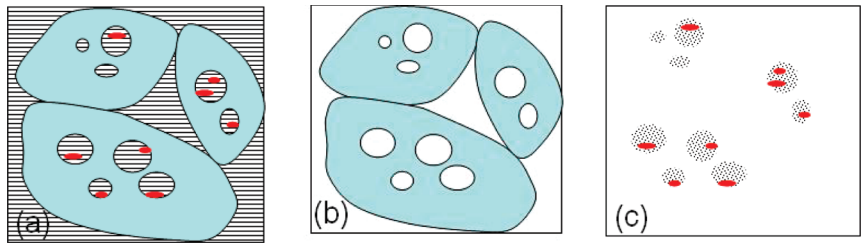

Figure 1. Schematic representations of neutron scattering contrast (relative scattering length density) maps of (a) carbon powder system (under the hydrogen pressure) comprised of the carbon grains (light blue), the excess adsorbed hydrogen (red), and the hydrogen gas (lines) confined in the pores (inside the carbon grain) and the voids (between the carbon grains) and (b) the carbon powder system under vacuum. Panel c is the subtraction of b from a, showing the strong scattering from excess adsorbed hydrogen and the weak scattering from hydrogen gas confined in the pores (the void contributions in the large Q range of SANS profile can be neglected here).

characterize the different scales of pore structures of AC used here. A high-pressure sample cell was especially designed and built to facilitate the pressure-dependent SANS measurements up to the hydrogen pressure of 1500 psi. The spatial distributions of hydrogen molecules physisorbed at RT corresponding to different storage capacities are correlated to the 3D confinement of nanospace in AC.

Experimental Methods

The SANS experiment was performed using 30 m SANS instrument at NG-7 of the National Institute of Standard and Technology (NIST) Center for Neutron Research (NCNR). An incident neutron beam has an average wavelength of 5 Å with a wavelength dispersion ($\Delta\lambda/\lambda_0$) of 12.5%. The AC powder sample used for the SANS study has a BET specific surface area (SSA) and micropore volume of 1457 m^2/g and 0.746 cm^3/g, respectively. This carbon sample contains 0.7 wt % of Pt metal. The details of the material synthesis have been described in the literature.[18] The contribution to the SANS signal by Pt metal can be ignored due to its low number density. Prior to SANS measurement, the sample was heated at 200 °C for 5 h under low vacuum (10^{-5} Torr) to remove the residual gas and adsorbed water. The carbon sample for SANS measurement was then sealed in a high pressure cell that is linked to a hydrogen gas tank through a stainless line. The gas pressure in the cell can be adjusted from 100 psi up to 1500 psi. The SANS experiments were performed by following hydrogen adsorption/desorption isotherm at RT. The excess adsorption capacities of carbon sample at various hydrogen pressures were obtained using in situ neutron transmission measurement. The results obtained from this neutron scattering method agrees with the results obtained with a traditional method.[18]

In the current study, the SANS profiles corresponding to various excess adsorption capacities at different pressures were collected with a counting time of 1 h after the transmission measurement step. The neutron measurements were performed after the hydrogen gas inside the pressure cell reached equilibrium. Each complete SANS scattering pattern was obtained through three SANS instrument configurations to cover the wide range of scattering vector Q from 0.007 to 0.33 $Å^{-1}$. The SANS profile of the carbon sample under vacuum was first collected as a background spectrum before charging the sample with hydrogen gas. This background spectrum was then analyzed to extract the information of the pore structure of our carbon sample. The bare carbon material (under vacuum) was also measured using the SANS instrument at the Oak Ridge National Laboratory (ORNL) to extend the high-Q range up to 0.7 $Å^{-1}$ so that the ultramicroporosity (less than 1 nm pore size) can be evaluated. Nitrogen sorption isotherms at 77 K were also performed using Micromeritics ASAP2020 to determine the pore size distribution, which is further compared with that obtained by SANS.

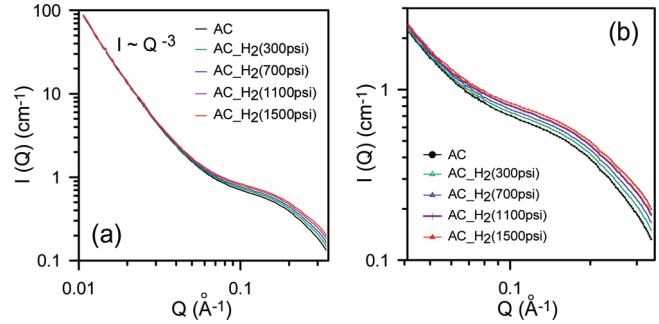

Figure 2. (a) Selected pressure-dependent SANS profiles for the AC sample under hydrogen adsorption isotherm, staring from the vacuum case. (b) Detailed variation of SANS profiles (of a) with hydrogen pressure in the high-Q region (0.04−0.33 $Å^{-1}$).

Results and Discussion

The hydrogen gas in our pressure cell can be divided into two parts: (1) the excess hydrogen adsorption (physisorption) in the micropores (inside the carbon grain) with the size of nanometers and (2) the hydrogen gas confined in the micropores and the voids (between the carbon grains) of the order of micrometers. Figure 1a,b shows the schematic representation of the carbon system with and without hydrogen, respectively. The voids of the order of micrometers (in Figure 1) do not contribute to the measured SANS profiles in the Q range indicated. Figure 2 shows the pressure-dependent SANS profiles selected (corresponding to Figure 1a) and that under the vacuum (corresponding to Figure 1b), respectively. Because of the existence of adsorbed hydrogen, it is not a simple two-phase problem for SANS structural characterization. This can be seen by the fact that increasing the hydrogen gas density by applying pressure does not result in a linearly proportional increase of the whole SANS profile. On the contrary, the SANS profiles mainly show a local variation in the high-Q region (0.05−0.33 $Å^{-1}$). This local variation as shown in Figure 2b corresponds to the newly formed nanoscale structure. It is worth pointing out that the coherent scattering length densities of the solid-state carbon (skeletal density = 2.23 g/cm^3), the vacuum, the hydrogen gas of 1000 psi, and the excess adsorbed hydrogen (assuming liquidlike) are estimated to be about 7.43×10^{-6} $Å^{-2}$, 0, -0.12×10^{-6} $Å^{-2}$, and -1.56×10^{-6} $Å^{-2}$, respectively. The rate of change of the square of coherent scattering length contrast caused by the hydrogen gas might be ignored as compared to that caused by the physisorbed hydrogen.

The pore structure of AC with a high SSA was reported to consist of spherical micropores (<2 nm in size) and a fractal

network formed by mesopore channels (>2 nm in width).[16] The large fractal dimension implies the nearly space-filling fractal networks in AC. In the literature,[16] the SANS intensity $I(Q)$ scattered from both (1) the fractal network of mesopore channels with the fractal dimension D_P and the channel width L_{ch} and (2) the spherical micropores with the diameter D_{micro} is expressed as follows:

$$I(Q) = I_P[1 + (QL_{ch}/2)^{-D_P}] \exp(-Q^2{L_{ch}}^2/20) + I_0 \exp(-Q^2{D_{micro}}^2/20) \quad (1)$$

where I_P and I_0 are related to the volume fractions of pore-fractal structures and micropores, respectively. The first term describes the fractal channel network contributing to the scattering profile in the intermediate- and low-Q region. In particular, the exponent associated with a power law decay at low Q range is typically related to the fractal dimension. The exponential expression of the second term is the Guinier approximation for the micropores, which mainly contributes to the scattering in the high-Q region. In eq 1, the correlation between micropore and mesopore is neglected.

The general literature[15] points out that the practical geometry of micropore is disklike. The second term of eq 1 is a Guinier approximation for the micropore, only applicable in the limited Q range. For accurately modeling the geometry of micropore in the entire measured Q range, the second term of eq 1 can be replaced by the proper form factor of cylinder. Usually, the scattering intensity due to a cylinder is given by

$$I(Q)_{cylinder} = \Delta\rho^2(\pi R^2 H) \int_0^{\pi/2} \times \left[2j_0\left(\frac{QH}{2}\cos\alpha\right)\frac{j_1(QR\sin\alpha)}{(QR\sin\alpha)}\right]^2 \sin\alpha\, d\alpha \quad (2)$$

where $\Delta\rho$ denotes the scattering length density contrast of the cylinder, R is the radius of the cylinder, and H is the height of the cylinder. The integral over α averages the form factor over all possible orientations of the cylinder with respect to Q. Therefore, eq 1 can be modified as

$$I(Q) = I_P[1 + (QL_{ch}/2)^{-D_P}] \exp(-Q^2{L_{ch}}^2/20) + I_1 \int_0^{\pi/2} \left[2j_0\left(\frac{QH}{2}\cos\alpha\right)\frac{j_1(QR\sin\alpha)}{(QR\sin\alpha)}\right]^2 \sin\alpha\, d\alpha \quad (3)$$

For thin disklike or near two-dimensional particles, eq 2 can also be approximated as[20]

$$I(Q)_{disk} \propto \frac{1}{Q^2}\exp(-Q^2T^2/12) \quad (4)$$

The above approximation is valid in the Q region (roughly, $\pi/R \ll Q \ll 2\pi/T$). T denotes the thickness of disklike particles. When $\ln[I(Q) \times Q^2]$ vs Q^2 is plotted, the SANS data concerning disklike particles fall on a straight line in the mentioned Q region. This type of plot is often used to examine the characteristics of disk particles. The thickness of disk can be model independently determined from the slop of this straight line ($= -T^2/12$). On the other hand, for thin rodlike or near one-dimensional particles, eq 2 can be approximated as[20]

$$I(Q)_{rod} \propto \frac{1}{Q}\exp(-Q^2R^2/4) \quad (5)$$

The above approximation is valid in the Q region (roughly, $2\pi/L \ll Q \ll \pi/R$). Similarly, the plot of $\ln[I(Q) \times Q]$ vs Q^2 for rodlike particles fall on a straight line in the mentioned Q region. This type of plot is often used to examine the characteristics of rod particles. The radius of rod can be model independently determined from the slop of this straight line ($= -R^2/4$).

As shown in Figure 3a, the SANS profile of pure AC sample (measured under vacuum) shows two power law regions. This SANS profile with the high-Q range up to 0.7 Å^{-1} was measured at ORNL and is consistent with that obtained at NIST. The feature of power law scattering in the low-Q region indicates the fractal network of the mesopore channel. In the high-Q region, the scattering curve showing a power law decay with the exponent of -2 represents the disklike geometry of micropores. The SANS data of pure AC sample can be well-fitted using the model of eq 3. The result of model fitting shows that the fractal dimension and channel width of mesopore network are 3.0 and 2.1 nm, respectively. The thickness of disklike micropore is ~0.4 nm. According to the model-independent method of eq 4, the mean thickness of micropores is also determined to be about 0.5 nm from the slope of the straight line in the plot of $\ln[I(Q) \times Q^2]$ vs Q^2 (Figure 3b). Both results are close to each other. Additionally, $\ln[I(Q) \times Q]$ vs Q^2 was also plotted in Figure 3b to confirm the validity of the used plot, $\ln[I(Q) \times Q^2]$ vs Q^2, for disklike geometry. The pore size used in nitrogen isotherm analysis and simulation works is usually defined as the distance between atomic centers of the opposite walls. For comparison, the thickness values of disklike micropre determined by both SANS analyses are corrected as 0.6 and 0.7 nm. The SANS method has a defect in this case. It cannot identify the polydispersity on the radius or thickness of micropores. The SANS method equally detects all pores, including the closed pores and open pores. In contrast, the nitrogen isotherm analysis is only sensitive to the open pores of interest (also accessible by hydrogen molecules). It analyzes the pore size (width) distribution assuming the slitlike geometry. The nonlocal density functional theory (NLDFT) model of nitrogen isotherm analysis shows the pore width distribution with multiple peaks at 0.6, 0.8, 1.2, and 1.5 nm, respectively. The Horvath−Kawazon (HK) model shows a different result, a broadening distribution with a single peak at 0.55 nm (Supporting Information). In conclusion, the pore size of majority of open micropore is 0.6 nm. The other sizes in minor are 0.8, 1.2, and 1.5 nm, respectively.

As mentioned, the variation of SANS profiles of Figure 2b signifies the formation of a new structure due to the excess hydrogen adsorption. Figure 1c illustrates the neutron scattering contrast map corresponding to the subtraction of Figure 1b from Figure 1a, showing the strong scattering from excess adsorbed hydrogen and the weak scattering from hydrogen gas confined (the latter can be neglected in the discussion of the first paragraph). It explains that the SANS profile of the AC sample under vacuum subtracted from that under hydrogen pressure can yield the SANS profile purely resulting from the structure of physisorbed hydrogen. It can be regarded as an approximate approach and is found in the other cases, such as carbon-supported nanoparticle (Supporting Information). For accurately analyzing the SANS profile due to the formation of local hydrogen distribution, the subtraction due to the pressure-dependent incoherent scattering background of hydrogen was

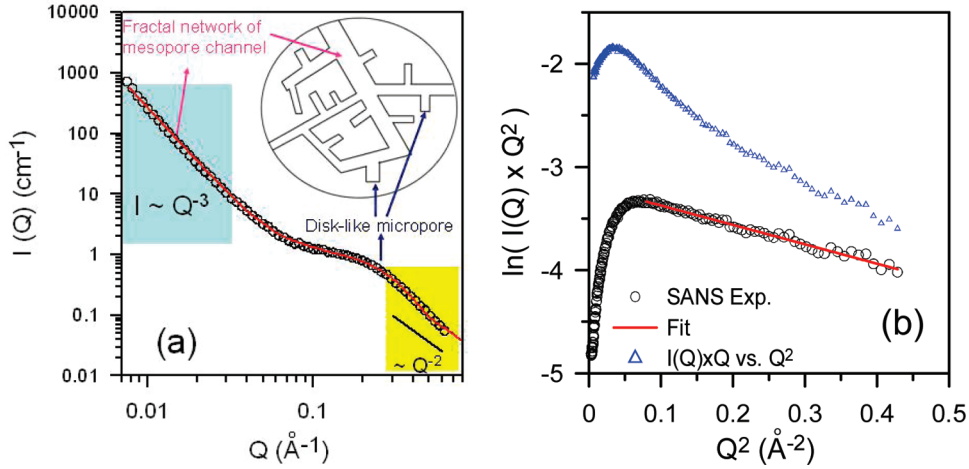

Figure 3. (a) Comparison of the measured SANS profile (empty circle) of the pure AC sample with the fitted intensity (red lines) using the model of the fractal network of mesopore channel and disklike micropore. (b) Kracty−Porod plot, $I(Q) \times Q^2$ vs Q^2, of the measured SANS profile in panel a, the slope of which gives to the thickness of the disklike micropores. The other plot [$I(Q) \times Q$ vs Q^2; blue triangle] for the thin rod form is shown for a comparison.

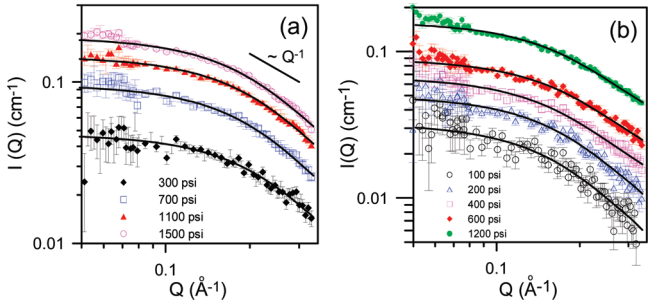

Figure 4. (a) SANS profiles resulted from the physisorbed hydrogen of of Figure 2b after the data treatment of various subtractions. Solid lines are the fitted curves. (b) Similar SANS profiles corresponding to the AC sample under the increasing hydrogen pressure (100 and 200 psi) and the decreasing hydrogen pressure (1200, 600, and 400 psi).

made here (Supporting Information). After the data treatment, including the subtractions of various contributions, the SANS profile of the AC sample under vacuum, the fitting of power law scattering in the low-Q region, and the constant incoherent scattering background, the SANS profiles resulted from the physisorbed hydrogen of Figure 2b are shown in Figure 4a. For the other hydrogen isotherm at RT of the AC sample, some SANS profiles under the increasing hydrogen pressure and the decreasing hydrogen pressure were selected and processed with the same data treatment mentioned above. Similar SANS profiles due to the physisorbed hydrogen corresponding to the selected pressures of adsorption and desorption are shown in Figure 4b.

The SANS profiles shown in Figure 4 have a rough power law scattering [$I(Q) \propto Q^{-1}$] in the high-Q region. This feature suggests that the structure formed by the excess hydrogen adsorption is cylinder-like. These SANS profiles can be fitted well using the cylinder form factor of eq 2, as shown in Figure 4. The computer program for model analysis was developed by the SANS group of NCNR.[21] The model-fitting result shows that the diameter and length of the cylinder approximation are 0.5−0.7 and 2.4−2.7 nm, respectively (Supporting Information). On the other hand, the plots of $\ln[I(Q) \times Q]$ vs Q^2 (Kractky−Porod plots) were made to examine the rodlike characteristics, as shown in Figure 5. The diameter model independently determined by the slope of straight line (Figure 5) and eq 5 is 0.5−0.6 nm. Herein, the straight line is in the limited Q range but can be reasonably regarded to linearly extend to the very high-Q region. The key parameter is the slope of the straight line. It seems that the method of Kractky−Porod plot is less sensitive to the lack of the SANS intensity profile in the high-Q region. Both results on the determination of diameter are close to each other, except for the SANS data at 100 and 200 psi with larger deviation [Figure 5b and in the high-Q region (Figure 5a)]. In conclusion, the diameter of cylinder approximation is intermediate between 0.5 and 0.6 nm. The cylinder length is in the order of the diameter of disklike micropore. The SANS analysis indicates that the sizes and the neutron contrasts of the cylinder structures at different hydrogen pressures or the hydrogen storage capacities vary so slightly that they can be regarded as the same. However, the volume fraction (or particle number density) of this kind of cylinder as a basic particle almost linearly varies with the hydrogen pressures from 100 to 1500 psi (corresponding to the hydrogen storage capacities from 0.09 to 0.5 wt %) (Supporting Information).

Although the SANS analysis provides an approximated result for the cylinder structure, we try to schematically understand whether the cylinder structure formed by the hydrogen molecules physisorbed on the carbon plan (graphene) is reasonable. The adsorption energy of hydrogen on pristine grapheme is a function of pore width for slitlike geometry. In the smallest pores of 0.6−0.7 nm in width, the adsorption energy is maximal, but only one layer of hydrogen can be accommodated.[10] For the pore width of 0.9−1.2 nm, adsorption of only two layers occurs on the carbon walls at RT based on the theoretical calculation. In this work, for most of the micropores (pore width of ~0.6 nm), 3D distribution of physisorbed hydrogen in the disklike micropore (monolayer) is constructed according to the SANS analysis, as shown in Figure 6a. Red dashed lines show the approximation of a cylinder-like cluster (SANS result) formed by the linear aggregation of hydrogen molecules. The pore width is in the x-direction. A cross-section of cylinder lies on the $x-y$ plane. The length of the cylinder is along the y-direction (or the direction of pore diameter). Figure 6b illustrates how the hydrogen molecules adsorbed on the pore wall (graphene sheet) aggregate (closely pack) into a cylinder-like cluster (on the $x-z$ plane; top view). According to the literature, the diameter of hydrogen molecule is ~0.3 nm.[22] The minimum distance between hydrogen molecules adsorbed on the atomic plane can be estimated to be ~0.3 nm.[23] The distance between carbon atoms (center-to-center) of graphene is ~0.15 nm. Their zigzag array explains why the diameter of approximated cylinder cluster

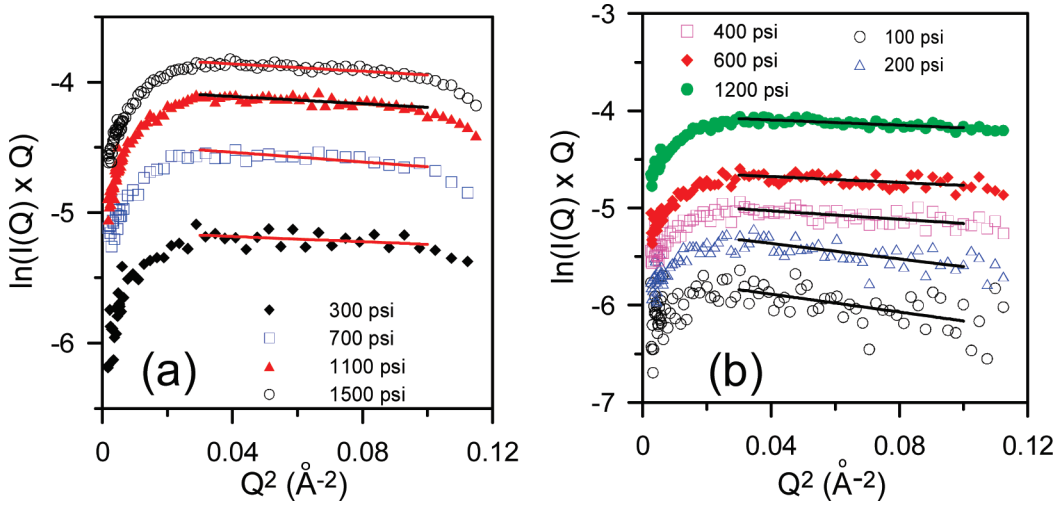

Figure 5. Kracty−Porod plots [$I(Q) \times Q$) vs Q^2], a and b, of the SANS profiles corresponding to Figure 4a,b, respectively. The slope of the fitted line gives the radii of the cylinder-like clusters formed by the excess adsorbed hydrogen.

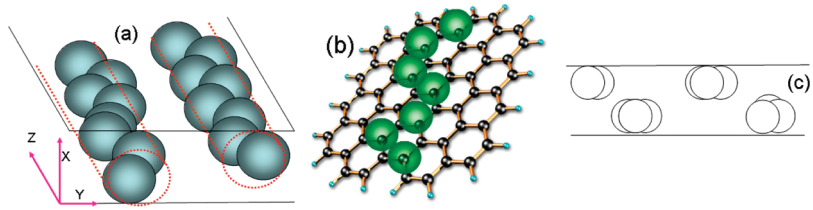

Figure 6. (a) 3D distribution of physisorbed hydrogen in the smallest disklike micropore (monolayer of the excess adsorbed hydrogen). The gray ball represents a hydrogen molecule. Dashed lines show the approximation of cylinder-like cluster formed by hydrogen aggregation. (b) Schematic representation of hydrogen molecules (green balls) adsorbed on the hexagonally packed graphene sheet (black balls represent carbon atoms). (c) Side view ($x-y$ plane) of 3D distribution of two layers of hydrogen confined in the micropore.

(∼0.5 nm) is slightly greater than that of hydrogen molecule (∼0.3 nm). The high neutron contrast also depicts the close packing between hydrogen molecules inside the cluster.

The SANS result fitted with simple cylinder form factor of few parameters provides the fact that a roughly line-shape cluster of aggregation of hydrogen molecules physisorbed on the graphene exists. Because there is no apparent structure peak in the SANS curves (in Figure 4), it can be conjectured that the spatial distribution of these clusters in the real disklike pore (pore width: 0.6−0.7 nm) is random and well-separated, as shown in Figure 6a. Note that the cluster number density linearly varies with the hydrogen pressure or excess adsorption capacity, but their spatial positions still keep no interaction with each other in the investigated pressures. According to the theoretical works,[13,14] the aggregated cluster of supercritical hydrogen and the other gas fuels at RT tend to be formed, depending on the balance of interaction energies of hydrogen−hydrogen in the space structure and on the surface characteristic of nanopores. Here, the SANS data interestingly show the directly experimental observation of this phenomenon. Figure 6c shows the side view ($x-y$ plane) of 3D distribution of two layers of hydrogen confined in the micropore (pore width, 0.9−1.2 nm) constructed from the basic cluster aggregated by hydrogen molecules. The behavior of structural evolution with hydrogen pressure is helpful to the study of adsorption mechanism of hydrogen at RT and high pressure and the material modification for enhancing the storage capacity.

It is found that the SANS profiles (Figure 4) can also be fitted well using a flexible cylinder form factor.[24] The related computer program was provided by NCNR.[21] This model is a parametrization of simulations of a discrete representation of the wormlike chain model of Kratky and Porod applied in the pseudocontinuous limit. The fitting result shows that the diameter of cylinder is ∼0.3 nm and is consistent with that of hydrogen molecule. The kuhn length (two times persistence length) is ∼0.6 nm. The contour length is 5.3 nm (Supporting Information). The fitting curve also coincides with that calculated from the cylinder form factor. The parameter of diameter is very sensitive among all fitting parameters because its contribution seems to dominate in the used Q region. Figure 7 shows the schematic representation of a more realistic hydrogen packing model described by the flexible cylinder model. This result also supports the deduction of line-shape aggregation of hydrogen.

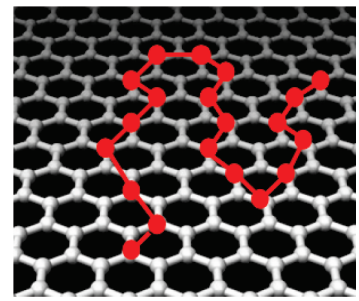

Figure 7. Schematic representation of hydrogen distribution on the carbon plane described by the SANS analysis using the flexible cylinder model.

Conclusion

We successfully establish the SANS technique for the determination of the aggregate structure and spatial distribution of hydrogen adsorbed in carbon nanopores at RT and high pressures. The hierarchical pore structure of AC is also studied by combining SANS and gas adsorption method. The SANS

result demonstrates that the fractal dimension, D, and the channel width, w, of the mesopore network are $D = 3.0$ and $w = 2.1$ nm, respectively. The main micropore is of disklike geometry with an average thickness of $t = 0.6$ nm. It is found for the first time that the cylinder-like clusters are formed by hydrogen aggregation. Two possible packing models for the clusters are proposed by the SANS analysis. This form of cluster can be regarded as a basic unit for the spatial distribution of hydrogen. Its structure is related to the 3D structure of micropores confining the hydrogen. The volume fraction of the clusters increases linearly with increasing hydrogen pressure up to 1500 psi (or the hydrogen storage capacity up to 0.5 wt %). The realistic 3D spatial distribution of hydrogen physisorbed in the micropore at RT is thus elucidated here. This experimental result thus provides a new basis for the future investigations of the RT storage mechanism of hydrogen in the nanoporous materials developed for the purpose of on-board hydrogen storage.

Acknowledgment. The research at MIT is supported by DOE Grants DE-FG02-90ER45429. We greatly appreciate technical assistance of Dr. Yun Liu during this experiment. We thank NIST Center for Neutron Research for allocation of neutron beam time in NG-7 SANS. C.-S.T. acknowledges the hospitality of the Department of Nuclear Science and Engineering of MIT during his stay as a Visiting Scientist.

Supporting Information Available: Pore width distributions determined by different models of nitrogen adsorption method, the discussion of intensity subtraction, the calculation of incoherent scattering background due to hydrogen, and the parameters determined by the model-fitting and model-independent methods, respectively. This material is available free of charge via the Internet at http://pubs.acs.org.

References and Notes

(1) Tollefson, J. *Nature* **2010**, *464*, 1262–1264.
(2) Wang, L.; Yang, R. T. *J. Phys. Chem. C* **2008**, *112*, 12486–12494.
(3) Tsao, C. S.; Tzeng, Y. R.; Yu, M. S.; Wang, C. Y.; Tseng, H. H.; Chung, T. Y.; Wu, H. C.; Yamamoto, K.; Kaneko, K.; Chen, S. H. *J. Phys. Chem. Lett.* **2010**, *1*, 1060–1063.
(4) Li, Y.; Yang, R. T. *J. Phys. Chem. C* **2007**, *111*, 11086–11094.
(5) Panella, B.; Hirscher, M.; Roth, S. *Carbon* **2005**, *43*, 2209–2214.
(6) Bhatia, S.; Myers, A. *Langmuir* **2006**, *22*, 1688–1700.
(7) Burress, J.; Kraus, M.; Beckner, M.; Cepel, R.; Suppes, G.; Wexler, C.; Pfeifer, P. *Nanotechnology* **2009**, 204026.
(8) Kuchta, B.; Firlej, L.; Pfeifer, P.; Wexler, C. *Carbon* **2010**, *48*, 223–231.
(9) Firlej, L.; Roszak, S.; Kuchta, B.; Pfeifer, P.; Wexler, C. *J. Chem. Phys.* **2009**, *131*, 164702.
(10) Kuchta, B.; Firlej, L.; Cepel, R.; Pfeifer, P.; Wexler, C. *Colloids Surf., A* **2010**, *357*, 61–66.
(11) Ohba, T.; Nicholson, D.; Kaneko, K. *Langmuir* **2003**, *19*, 5700–5707.
(12) Suzuki, T.; Kaneko, K.; Gubbins, K. E. *Langmuir* **1997**, *13*, 2545–2549.
(13) Ohba, T.; Omori, T.; Kanoh, H.; Kaneko, K. *J. Phys. Chem. B* **2004**, *108*, 27–30.
(14) Murata, K.; Kaneko, K.; Kanoh, H.; Kasuya, D.; Takahashi, K.; Kokai, F.; Yudasaka, M.; Lijima, S. *J. Phys. Chem. B* **2002**, *106*, 11132–11138.
(15) Rodriguez-Reinoso, F. *Carbon* **1998**, *36*, 159–175.
(16) Pfeifer, P.; Ehrburger-Dolle, F.; Rieker, T. P.; Gonzalez, M. T.; Hoffman, W. P.; Molina-Sabio, M.; Rodriguez-Reinoso, F. P.; Schmidt, W.; Voss, D. *Phys. Rev. Lett.* **2002**, *88*, 115502−1–4.
(17) Neumann, D. A. *Mater. Today* **2006**, *9*, 34–41.
(18) Tsao, C. S.; Liu, Y.; Li, M.; Zhang, Y.; Leao, J. B.; Chang, H. W.; Yu, M. S.; Chen, S. H. *J. Phys. Chem. Lett.* **2010**, *1*, 1569–1573.
(19) Tsao, C. S.; Chen, C. Y.; Chung, T. Y.; Su, C. J.; Su, C. H.; Chen, H. L.; Jeng, U. S.; Yu, M. S.; Liao, P. Y.; Lin, K. F.; Tzeng, Y. R. *J. Phys. Chem. C* **2010**, *114*, 7014–7020.
(20) Glatter, O.; Kratky, O. *Small-Angle X-Ray Scattering*; Academic Press: London, 1982.
(21) Kline, S. R. *J. Appl. Crystallogr.* **2006**, *39*, 895–900.
(22) Düren, T.; Millange, F.; Férey, G.; Walton, K. S.; Snurr, R. Q. *J. Phys. Chem. C* **2007**, *111*, 15350–15356.
(23) Liu, Y.; Kabbour, H.; Brown, C.; Neumann, D. A.; Ahn, C. C. *Langmuir* **2008**, *24*, 4772–4777.
(24) Pedersen, J. S.; Schurtenberger, P. *Macromolecules* **1996**, *29*, 7602–7612.

JP1055039